Helical filaments

Nicholas Barbieri, Zahra Hosseinimakarem, Khan Lim, Magali Durand, Matthieu Baudelet, Eric Johnson, and Martin Richardson

Citation: Applied Physics Letters **104**, 261109 (2014); doi: 10.1063/1.4886960
View online: http://dx.doi.org/10.1063/1.4886960
View Table of Contents: http://scitation.aip.org/content/aip/journal/apl/104/26?ver=pdfcov
Published by the AIP Publishing

Helical filaments

Nicholas Barbieri,[1] Zahra Hosseinimakarem,[2] Khan Lim,[1] Magali Durand,[1] Matthieu Baudelet,[1] Eric Johnson,[2] and Martin Richardson[1]
[1]*Townes Laser Institute, CREOL—The College of Optics and Photonics, University of Central Florida, Orlando, Florida 32816, USA*
[2]*Micro-Photonics Laboratory – Center for Optical Material Science, Clemson, Anderson, South Carolina 29634, USA*

(Received 28 May 2014; accepted 22 June 2014; published online 1 July 2014)

The shaping of laser-induced filamenting plasma channels into helical structures by guiding the process with a non-diffracting beam is demonstrated. This was achieved using a Bessel beam superposition to control the phase of an ultrafast laser beam possessing intensities sufficient to induce Kerr effect driven non-linear self-focusing. Several experimental methods were used to characterize the resulting beams and confirm the observed structures are laser air filaments. © *2014 AIP Publishing LLC*. [http://dx.doi.org/10.1063/1.4886960]

Laser filamentation in air is a nonlinear phenomenon that occurs for ultrafast laser pulses with peak powers in excess of a critical power ~3 GW. It arises primarily from two nonlinear processes. First, modification of the refractive index of air by optical Kerr effect causes the beam to self-focus, overcoming normal diffraction.[1,2] When intensities of 10^{13} W/cm^2 are achieved, ionization of the propagation medium provides a compensating negative refractive index, causing the beam to stabilize into a ~100 μm (full-width half maximum (FWHM)) diameter plasma filament,[3–6] i.e., a self-guided ionizing light channel that can propagate over several hundred meters.[2,5,7,8] Dynamic competition within the filament clamps the peak intensity at 3×10^{13} W/cm^2.[9,10] For powers several times greater than the filamentation critical power, multiple filamentation occurs.[11,12] The organization of these channels is based on the noise within the initial spatial profile of the beam and, if not controlled, can change on a shot-to-shot basis. Under these conditions, this phenomenon is unsuitable for applications that require control or consistency in the ordering of the filaments. However, ordered filament arrays can be obtained through appropriate modification of the laser wavefront prior to filamentation.[13–15]

The ability to control and order multiple filaments originating from a single laser beam is critical to expanding the range of practical application of laser filaments. In particular, filamentation provides a promising approach to guiding microwave radiation, either by synthesizing conventional guiding structures,[16–19] or by creating more unorthodox structures, such as the recently suggested virtual hyperbolic metamaterials.[20]

Non-diffracting beams[21–25] provide a promising means of controlling filamentation. Previous laboratory studies of the control of single filaments using non-diffracting beams have led to the observation of both Bessel filaments[26–29] and Airy filaments.[30,31] Non-diffracting beams are not limited to single peak intensity beams. Since Bessel beams are a basis of the Helmholtz equation,[32] beams of any geometry can be obtained through the suitable superposition of Bessel beams, including beams with multiple intensity peaks.[33] We have previously demonstrated dual, helical non-diffracting beams[34] using this approach.

In the present paper, the creation of dual helical filaments in air is demonstrated. These beams extend over distances of 2 m in the laboratory and possess the ionization, self-cleaning and spectral broadening properties associated with air filaments. These experiments demonstrate the use of non-diffractive beams as a means of generating ordered arrays of filaments in air.

The laser system used was an ultrafast Ti:sapphire laser system providing 800 nm pulses with a pulse duration of 50 fs at 10 Hz and energies up to 20 mJ. The beam had a 10 mm (FWHM) Gaussian spatial profile. Helical beams were generated by placing a complex coaxial vortex plate (VP) in series with a pair of coaxially aligned Fresnel axicons (AX) along the laser propagation axis (Fig. 1). The complex coaxial vortex plate comprised an inner vortex plate 5 mm in diameter that induced a unit azimuthal charge onto the 800 nm beam, and a surrounding 10 mm diameter phase plate that induced the opposite azimuthal charge on the beam. The Fresnel axicon phase plate featured two separate cone angles. Within the inner diameter of 5 mm, the axicon refracted light at an angle of 0.0375°, while light outside this diameter was refracted at an angle of 0.0625°.

Helical beams are obtained from the superposition of two first order Bessel-Gauss beams of opposite azimuthal charge. First order Bessel beams can be generated by placing an axicon and an azimuthal phase plate in series with a Gaussian beam.[34,35] The aforementioned setup operates by generating two Bessel beams in series by applying different axicon angles and azimuthal phases at different distances from the optical axis, and permitting the resulting beams to interfere along the optical axis during propagation.

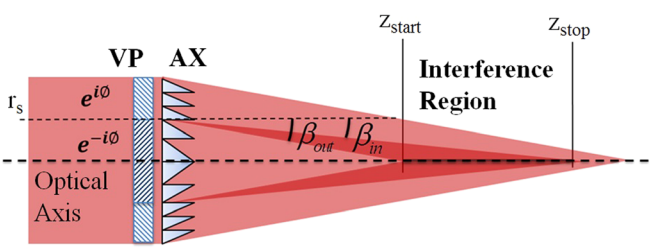

FIG. 1. Configuration for double helical filament formation.

This configuration (Fig. 1) can be modeled by applying the phase lag associated with the axicons and the vortex phase plate to the incident Gaussian beam. For $r < r_s$, the associated phase lag is

$$E_{inner} = \exp(-i\phi)\exp(-ik\beta_i r)E_{incident}, \tag{1}$$

while for $r > r_s$ the associated phase lag is

$$E_{outer} = \exp(i\phi)\exp(-ik\beta_o r)E_{incident}. \tag{2}$$

Substituting these expressions into the Fresnel diffraction integral for the $\lim\beta_i \rightarrow \beta_o$ and calculating the resulting intensity from the corresponding diffracted electric field yields

$$I(r,\phi,z) = I_0 C(z) J_1^2(k_{\perp,o} r)\cos^2[\theta(\phi,z)], \tag{3}$$

where

$$C(z) = 4\pi\frac{k_\perp^2 z}{2k}\exp\left(-\frac{2z^2}{l_{df,o}^2}\right) \tag{4}$$

and

$$\theta(\phi,z) = \phi - \frac{k_{\perp,o}^2 - k_{\perp,i}^2}{4k}z. \tag{5}$$

Here, k is the wavenumber, $k_{\perp,o} = \beta_o k$, $k_{\perp,i} = \beta_i k$, and $k_\perp = k\beta$, where $\beta = (\beta_o + \beta_i)/2$, the transverse wavenumbers associated with the outer and inner regions of the axicons and $l_{df,o} = w/\beta_o$, where w is the Gaussian beam waist of the incident beam. The angles β_i and β_o are the axicon refraction angles associated with $r < 2.5$ mm and $r > 2.5$ mm, respectively. Because of the z dependence of Eq. (5), the beam intensity profile rotates during propagation at a rate

$$\frac{\partial\theta}{\partial z} = \frac{k_{\perp,o}^2 - k_{\perp,i}^2}{4k} = \frac{\pi}{2}\frac{\beta_o^2 - \beta_i^2}{\lambda}. \tag{6}$$

The size of the helical beam can be estimated from Eq. (3). Observing that each intensity peak is bounded by the first and second zeros of $J_1(k_{\perp,o}r)$, the diameter of the individual intensity peaks cannot exceed

$$d_{max} = \frac{3.8317}{k_\perp} = \frac{1.22\lambda}{\beta_o + \beta_i}. \tag{7}$$

The spacing of the helical beam intensity peaks can similarly be estimated. Assuming each intensity peak is centered on the first extremum of $J_1(k_{\perp,o}r)$, and observing that the cosine term in Eq. (3) requires an azimuthal separation of π, then the center of the intensity peaks are separated by a distance of

$$d_{sep} = \frac{3.6824}{k_\perp} = \frac{1.17\lambda}{\beta_o + \beta_i}. \tag{8}$$

In our experimental case, the diffraction angles were set at $\beta_i = 0.0375°$ and $\beta_o = 0.0625°$. Substituting these values into the above equations give a rotation rate of $\partial\theta/\partial z = 0.015$ rad/cm or 0.86 deg/cm, a maximum beam diameter of $d_{max} = 560\,\mu$m and a beam separation value of $d_{sep} = 540\,\mu$m.

The peak intensity can be calculated by evaluating Eq. (3) at $r = d_{sep}/2$ and $\phi = (k_{\perp,o}^2 - k_{\perp,i}^2)z/4k$, yielding

$$I(z) = 23\left(\frac{\beta^2}{\lambda}\right)z\exp\left(-\frac{2z^2}{l_{df,o}^2}z\right)I_0. \tag{9}$$

Using calculus, this intensity distribution can be shown to peak at $z = l_{df,o}/2$, for which the above equation reduces to

$$I = 6.94\frac{\beta w}{\lambda}I_0. \tag{10}$$

The initial Gaussian beam has an instantaneous on-axis intensity of $I_0 = E/8\tau w^2$, where E is the pulse energy and w is the beam waist. For $w = 8.0$ mm, a temporal pulse width of $\tau = 50$ fs and the pulse energies of 135 μJ and 11.5 mJ used in the experiment peak intensities of 5.27×10^8 W/cm^2 and 4.49×10^{10} W/cm^2 are obtained, respectively. Further substituting these intensity values into Eq. (10) along with $\lambda = 800$ nm and the axicon refraction angle yields peak on axis intensities associated with the helical beams of 0.46 TW/cm^2 for 135 μJ pulses and peak intensity of 39 TW/cm^2 for 11.5 mJ pulses.

The beam diffraction was also evaluated numerically. The Fresnel diffraction integral is given by

$$E_2(u,v,z) = \frac{e^{ikz}}{i\lambda z}\exp\left[\frac{i(u^2+v^2)}{4K}\right]T(x_1,y_1), \tag{11}$$

where

$$T(x_1,y_1) = \mathcal{F}[E_1(x_1,y_1,0)\exp[iK(x_1^2+y_1^2)]] \tag{12}$$

and $K = k/2z$, $u = 2Kx_2$, and $v = 2Ky_2$. This integral was evaluated using a fast-Fourier transform within MATLAB. To simulate the experiment, space resolved phase lags were used to model the experimental setup and applied to an incident Gaussian beam. The results of this simulation are shown in Fig. 2(a).

Helical filament experiments were first performed at low pulse energies (135 μJ) corresponding to a peak instantaneous laser power of 2.1 GW. This power level is below the critical power for filamentation.[1] The transverse profile of the beam was recorded at incremental distances from the beam synthesizer, which shows the expected beam rotation and beam fluence measurements as a function of distance[34] (Fig. 2(b)).

A helical beam composed of two isolated, rotating, elliptical spots was obtained over an extended distance of 2–4 m as measured from the coaxial axicon pair. The helical beams rotated at a constant rate of rotation of 0.875 deg/cm $\pm$0.025 deg/cm, which is consistent with both theory and simulation. The observed intensity spots are spaced $500 \pm 50\,\mu$m apart, possess a minor diameter of $175 \pm 50\,\mu$m and a major diameter of $350 \pm 150\,\mu$m. The location, size, and rotation rate of these intensity spots are reproduced by the simulation (Fig. 2(a)).

Helical filament propagation was then investigated at laser power levels of 180 GW, above the threshold for filament formation. Verification of filament formation in these tests was made by detection of air ionization and spectral

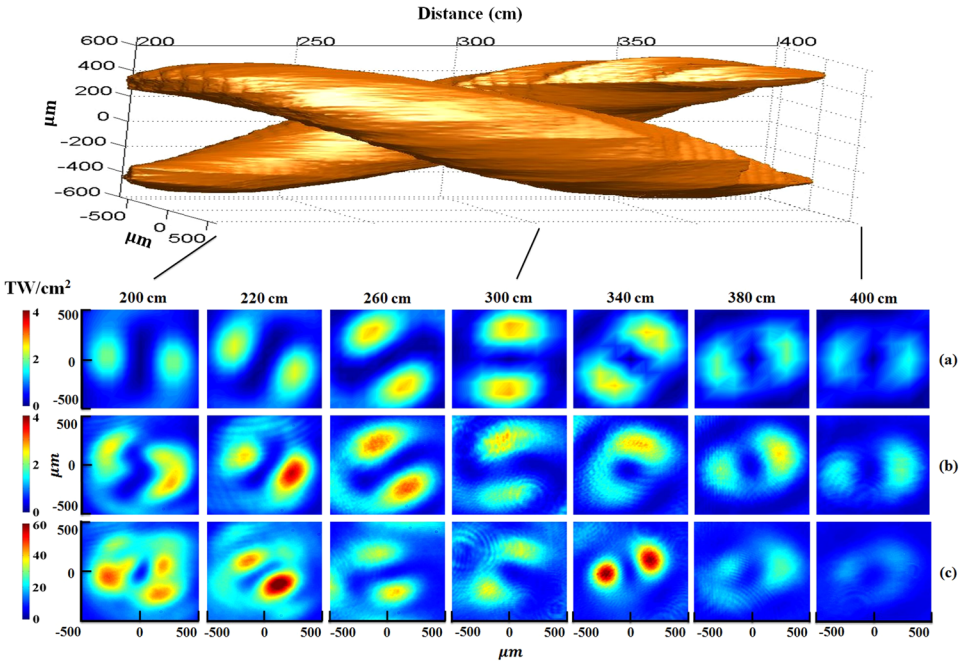

FIG. 2. Top: An isometric rendering of the intensity iso-surface of the helical beam as it propagates through space (as taken from simulation). Bottom: Helical beam transverse profiles as a function of propagation distance, simulated (a), measured for 135 μJ pulses (b) and 11.5 mJ pulses (c).

broadening, both occurring for intensities above 10^{13} W/cm^2. To measure ionization, a pair of 20 mm × 25 mm copper electrodes spaced 12 mm apart, and raised to a potential of 8.5 kV using a capacitive driver circuit[26,28] was located symmetrically about the propagating helical beam. An oscilloscope recorded the voltage drop across a 6 MΩ resistor placed in series with the cathode. The maximum value of this voltage drop was then averaged over 10 shots recorded at each point, and the standard deviation was taken as the error (Fig. 3).

At laser pulse energies of 11.5 mJ, the helical beams are observed to ionize over a distance of 160 cm–380 cm as measured from the axicon. Both the beam peak intensity and the ionization signal strength display two longitudinally separated peaks. These peaks show approximate correspondence, with the first ionization peak preceding the first intensity peak by 30 cm while the second ionization peak occurs 10 cm beyond the second intensity peak.

The helical filament transverse profiles taken over the ionizing region are shown in Fig. 2(c). When compared to the linear case, the helical filaments maintain the same basic structure and energy distribution. The beams retain their general shape and continue to rotate at a constant rate of 0.875 deg/cm, but undergo a 20° angular shift relative to their linear counterparts. The largest differences are observed for the images taken at 220 cm and 340 cm (Fig. 2(c)), which are located at the two intensity peaks of this helical beam (Fig. 3). Several effects are observed at these points, including a reduction in the spacing between the two helical beam spots by 63 – 125 μm, a reduction in the diameter of each spot, an increase in beam peak intensity and an improvement in beam quality indicating the helical filaments were undergoing spatial cleaning.[36,37] At 340 cm, the helical beam peaks transform from elliptical spots to circular spots measuring 175 μm in diameter, further demonstrating the effects of spatial cleaning on the helical filament.

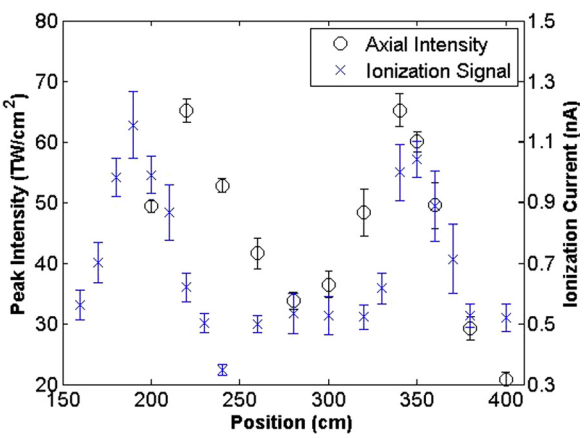

FIG. 3. Ionization signal strength and simulated intensity as a function of beam propagation distance.

The modifications to helical beam shape and rotation rate mirror those predicted by Xi *et al.*[38] and later observed by Shim *et al.*[39,40] for the interaction between single laser filaments in air. When two filaments are spaced less than a millimeter apart, the superposition of their peripheral fields will modify the nonlinear effects governing light propagation. If the peripheral fields are in phase, the refractive index of the intervening space between the two filaments will increase, resulting in a mutual attracted between the filaments, as is being observed for the helical filaments. Additionally, if a small angle is present between the directions of propagation of the two filaments while they are interacting, the filament arrangement will also rotate in space by a finite angle. This is an effect which can clearly be observed in Fig. 2 for our experiment. Thus, both the consequence of laser filamentation and laser filament interaction have been observed from this experiment.

The spectrum associated with the helical filaments was recorded using two spectrometers (Ocean Optics USB2000 in the NIR and HR2000 in the visible) both prior to nonlinear propagation and after the helical filament had dissipated. The results are shown in Fig. 4. The measured spectrum was found to broaden, with amplitudes ≥1% increasing from

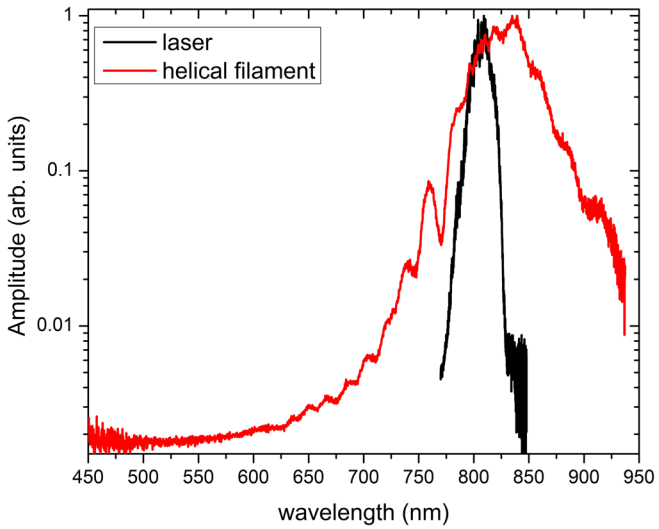

FIG. 4. Spectral broadening resulting from the filamentation of helical beams.

770–830 nm to 720–930 nm, consistent with the broadening observed for laser filamentation.[2,40,41]

By shaping an ultrafast pulse using a non-diffracting beam superposition, 2 m long helical filaments were formed in the laboratory. The beam size, spacing, and rotation rate were accurately described by our models, while the effects of both filamentation and mutual filament interaction were observed in the experimental results. These results demonstrate complex non-diffracting beam shapes can be used to control and shape laser filaments. With sufficient laser pulse energy, it should be possible to obtain other filament geometries using multi-intensity peaked non-diffracting beams, including cylindrical and rectangular arrays of filaments. Such filament structures would then be suitable for a variety of applications, including the generation and guiding of radio-frequency and microwaves.

The authors acknowledge useful discussions with Dr. D. Christodoulides, the support of Dr. M. Weidman and the funding support from the ARO MURI on Air Filamentation Science, the HEL JTO, the NCMR MASINT Program and the State of Florida.

[1]S. L. Chin, S. A. Hosseinim, W. Liu, Q. Luo, F. Theberge, N. Abozbek, A. Becker, V. P. Kandidov, O. G. Kosareava, and Schroeder, "The propagation of powerful femtosecond laser pulses in optical media: Physics, application, and new challenges," Can. J. Phys. **83**, 863–905 (2005).
[2]A. Couiaron and A. Mysyrowicz, "Femtosecond filamentation in transparent media," Phys. Rep. **441**, 47–189 (2007).
[3]H. D. Ladouceur, A. P. Baronavski, D. Lohrmann, P. W. Grounds, and P. G. Girardi, "Electrical conductivity of a femtosecond laser generated plasma channel in air," Opt. Commun. **189**, 107–111 (2001).
[4]S. Tzortzakis, M. A. Franco, Y.-B. Andre, A. Chiron, B. Lamouroux, B. S. Prade, and A. Mysyrowicz, "Formation of a conducting channel in air by self-guided femtosecond laser pulses," Phys. Rev. E **60**(4), R3505–R3507 (1999).
[5]B. La Fontaine, F. Vidal, Z. Jiang, C. Y. Chien, D. Comtois, A. Desparois, T. W. Johnston, J.-C. Kieffer, and H. Pepin, "Filamentation of ultrashort pulse laser beams resulting from their propagation over long distances in air," Phys. Plasmas **6**(5), 1615–1621 (1999).
[6]H. Yang, J. Zhang, Y. Li, J. Zhang, Y. Li, Z. Chen, H. Teng, Z. Wei, and Z. Sheng, "Characteristics of self-guided laser plasma channels generated by femtosecond laser pulses in air," Phys. Rev. E **66**, 016406 (2002).
[7]D. Faccio, A. Matijosius, A. Dubietis, R. Piskarskas, A. Varanavicius, E. Gaizauskas, A. Piskarskas, A. Couairon, and P. Di Trapani, "Near- and far-field evolution of laser pulse filaments in Kerr media," Phys. Rev. E **72**(3), 037601 (2005).
[8]M. Rodriguez, R. Bourayou, G. Mejean, J. Kasparian, J. Yu, E. Salmon, A. Scholz, B. Stecklum, J. Eisloffel, U. Laux, A. P. Hatzes, R. Sauerbrey, L. Woste, and J.-P. Wolf, "Kilometer-range nonlinear propagation of femtosecond laser pulses," Phys. Rev. E **69**, 036607 (2004).
[9]J.-F. Diagle, A. Jaron-Becker, S. Hosseini, T.-J. Wang, Y. Kamali, G. Roy, A. Becker, and S. L. Chin, "Intensity clamping measurement of laser filaments in air at 400 and 800 nm," Phys. Rev. A **82**(2), 023405 (2010).
[10]J. Kasparian, R. Sauerbrey, and S. L. Chin, "The critical laser intensity of self guiding light filaments in air," Appl. Phys. B **71**, 877–879 (2000).
[11]Z.-Q. Hao, J. Zhang, X. Li, T.-T. Xi, Y.-T. Li, X.-H. Yuan, Z.-Y. Zheng, Z.-H. Wang, W.-J. Ling, and Z.-Y. Wei, "Spatial evolution of multiple filaments in air induced by femtosecond laser pulses," Opt. Express **14**(2), 773–778 (2006).
[12]S. A. Hosseini, Q. Luo, B. Ferland, W. Liu, S. L. Chin, O. G. Kosareva, N. A. Panov, N. Akozbek, and V. P. Kandidov, "Competition of multiple filaments during the propagation of intense femtosecond laser pulses," Phys. Rev. A **70**, 033802 (2004).
[13]G. Mechain, A. Couairon, M. Franco, B. Prade, and A. Mysyrowicz, "Organizing multiple femtosecond filaments in air," Phys. Rev. Lett. **93**(4), 035003 (2004).
[14]G. Fibich, S. Eisenmann, B. Ilan, and A. Zigler, "Control of multiple filamentation in air," Opt. Lett. **29**(15), 1772–1774 (2004).
[15]M. Fisher, C. Sider, E. Johnson, O. Andrusyak, C. Brown, and M. Richardson, "Control of filamentation for enhancing remote detection with laser induced breakdown spectroscopy," Proc. SPIE **6219**, 621907 (2006).
[16]A. E. Dormidonov, V. V. Valuev, V. L. Dmitriev, S. A. Shlenov, and V. P. Kandidov, "Laser filament induced microwave waveguide in air," Proc. SPIE **6733**, 67332S (2007).
[17]M. Chateauneuf, S. Payeur, J. Dubois, and J.-C. Kieffer, "Microwave guiding in air by a cylindrical filament array waveguide," Appl. Phys. Lett. **92**, 091104 (2008).
[18]M. Alshershby, Z. Hao, and J. Lin, "Guding microwave radiation using laser-induced filaments: The hollow conducting waveguide concept," J. Phys. D: Appl. Phys. **45**, 265401 (2012).
[19]Y. Ren, M. Alshershby, Z. Hao, Z. Zhao, and L. Jingquan, "Microwave guiding along double femtosecond filaments in air," Phys. Rev. E **88**, 013104 (2013).
[20]Z. Kudyshev, M. C. Richardson, and N. M. Litchinitser, "Virtual hyperbolic metamaterials for manipulating radar signals in air," Nature Commun. **4**, 2557 (2013).
[21]J. Durnin and J. J. Miceli, Jr., "Diffraction-free beams," Phys. Rev. Lett. **58**(15), 1499–1501 (1987).
[22]Z. Bouchal, "Nondiffracting optical beams: Physical properties, experiments and applications," Czech. J. Phys. **53**(7), 537–578 (2003).
[23]D. McGloin and K. Dholakia, "Bessel beams: Diffraction in a new light," Contemp. Phys. **46**(1), 15–28 (2005).
[24]P. Polynkin, C. Ament, and J. V. Moloney, "Self-focusing of ultraintense femtosecond optical vortices in air," Phys. Rev. Lett. **111**, 023901 (2013).
[25]M. Fisher, C. Siders, E. Johnson, O. Andrusyak, C. B. Brown, and M. Richardson, "Control of filamentation for enhancing remote detection with laser induced breakdown spectroscopy," Proc. SPIE **6219**, 621907 (2006).
[26]P. Polykin, M. Kolesik, A. Roberts, D. Faccio, P. Di Trapani, and J. Moloney, "Generation of extended plasma channels in air using femtosecond Bessel beams," Opt. Express **16**(20), 15733–15740 (2008).
[27]D. Abdollahpour, P. Panagiotopoulos, M. Turconi, F. D. Jedrkiewicz, P. Di Trapani, A. Couairon, D. G. Papazoglou, and S. Tzortzakis, "Long spatio-temporally stationary filaments in air," Opt. Express **17**(7), 5052–5057 (2009).
[28]S. Akturk, B. Zhou, M. Franco, A. Couairon, and A. Mysyrowicz, "Generation of long plasma channels in air by focusing ultrashort laser pulses with an axicon," Opt. Commun. **282**, 129–134 (2009).
[29]P. Polynkin, M. Kolesik, and J. Moloney, "Extended filamentation with temporally chirped femtosecond Bessel-Gauss beams in air," Opt. Express **17**(2), 575–584 (2009).
[30]P. Polykin, M. Kolesik, J. V. Moloney, G. A. Siviglou, and D. N. Christodoulides, "Curved plasma channel generation using ultraintense airy beams," Science **324**, 229–232 (2009).
[31]P. Polynkin, M. Kolesik, and J. Moloney, "Filamentation of femtosecond laser airy beams in water," Phys. Rev. Lett. **103**, 123902 (2009).
[32]J.-Y. Lu, "Designing limited diffraction beams," IEEE Trans. Ultrason. Ferroelectr. Freq. Control **44**(1), 181–193 (1997).

[33]V. Arrizon, S. Chavez-Cerda, U. Ruiz, and R. Carrada, "Perioidic and quasi-periodic non-diffracting wave fields generated by superposition of multiple Bessel beams," Opt. Express **15**(25), 16748–16753 (2007).
[34]N. Barbieri, M. Weidman, G. Katona, M. Baudelet, Z. Roth, and E. Johnson, "Double helical laser beams based on interfering first-order Bessel beams," J. Opt. Soc. Am. A **28**(7), 1462–1469 (2011).
[35]J. Arlt and K. Dholakia, "Generation of high-order Bessel beams by use of an axicon," Opt. Commun. **177**, 297–301 (2000).
[36]B. Prade, M. Franco, A. Couairon, H. Buersing, B. Eberle, M. Krenz, and D. Seiffer, "Spatial mode cleaning by femtosecond filamentation in air," Opt. Lett. **31**(17), 2601–2603 (2006).
[37]A. Jarnac, M. Durand, A. Houard, Y. Liu, B. Prade, M. Richardson, and A. Mysyrowicz, "Spatiotemporal cleaning of a femtosecond laser pulse through interaction with counterpropagating filaments in air," Phys. Rev. A **89**(2), 023844 (2014).
[38]T.-T. Xi, X. Lu, and J. Zhang, "Interaction of light filaments generated by femtosecond laser pulses in air," Phys. Rev. Lett. **96**(2), 025003 (2006).
[39]B. Shim, S. E. Schrauth, C. J. Hensley, L. T. Vuong, P. Hui, A. A. Ishaaya, and A. L. Gaeta, "Controlled interaction of femtosecond light filaments in air," Phys. Rev. A **81**(6), 061803 (2010).
[40]J. Kasparian, R. Sauerbrey, D. Mondelain, S. Niedermeier, J. Yu, J.-P. Wolf, Y.-B. Andre, M. Franco, B. Prade, S. Tzortzakis, A. Mysyrowicz, M. Rodriguez, H. Wille, and L. Wöste, "Infrared extension of the supercontinuum generated by femtosecond terawatt laser pulses propagating in the atmosphere," Opt. Lett. **25**(18), 1397–1399 (2000).
[41]E. Schulz, D. S. Steingrube, T. Binhammer, M. B. Gaarde, A. Couairon, U. Morgner, and M. Kovacev, "Tracking spectral shapes and temporal dynamics along a femtosecond filament," Opt. Express **19**(20), 19495–19507 (2011).